Title: A machine learning approach to designing tough and degradable polyamides based on multiblock structures

Authors: Yoshifumi Amamoto[1,2,3]*, Chie Koganemaru[1], Ken Kojio[1,4], Atsushi Takahara[1,4], Sayoko Yamamoto[5], Kazuki Okazawa[1], Yuta Tsuji[1,5], Toshimitsu Aritake[6], Kei Terayama[7,8,9]*

Affiliations:

[1]Institute for Materials Chemistry and Engineering, Kyushu University, 744 Motooka, Nishi-ku, Fukuoka 819-0395, Japan

[2]Graduate School of Artificial Intelligence and Science, Rikkyo University, 3-34-1 Nishi-Ikebukuro, Toshima-ku, Tokyo 171-8501, Japan

[3]Graduate School of Social Data Science, Hitotsubashi University, 2-1 Naka, Kunitachi, Tokyo 186-8601, Japan

[4]Research Center for Negative Emission Technology, Kyushu University, 744 Motooka, Nishi-ku, Fukuoka 819-0395, Japan

[5]Faculty of Engineering Sciences, Kyushu University, 6-1, Kasuga-koen, Kasuga, Fukuoka, 816-8580, Japan

[6]Hitotsubashi Institute for Advanced Study, Hitotsubashi University, 2-1 Naka, Kunitachi, Tokyo 186-8601, Japan

[7]Graduate School of Medical Life Science Department of Medical Life Science, Yokohama City University, 1-7-29 Suehiro-cho, Tsurumi-ku, Yokohama, Kanagawa 230-0045, Japan

[8]RIKEN Center for Advanced Intelligence Project, 1-4-1 Nihonbashi, Chuo-ku, Tokyo

103-0027, Japan

[9]MDX Research Center for Element Strategy, Tokyo Institute of Technology, 4259 Ngatsuta-cho, Midori-ku, Yokohama, Kanagawa, 226-8501, Japan

*Correspondence: y.amamoto@r.hit-u.ac.jp (Y.A.); terayama@yokohama-cu.ac.jp (K.T.).

Abstract: The development of environmentally friendly plastics is receiving renewed attention for a sustainable society. The trade-off between toughness and degradability is one of the issues associated with biodegradable polymers, which prevents these materials from being broadly utilised. However, designing biodegradable polymers that overcome these issues is often difficult. In this study, we demonstrate that machine-learning techniques can contribute to the development of multiblock polyamides composed of Nylon6 and α-amino acid segments that are satisfactorily mechanically tough and degradable. Multi-objective optimisation based on Gaussian process regression suggested appropriate α-amino acid sequences for polyamides endowed with both properties. Physical factors associated with the sequence as well as higher-order multiblock-derived structures were revealed to be essential for endowing these polymers with satisfactory properties. Furthermore, these materials are degradable in natural muddy water. Our method provides a useful approach for designing and understanding environmentally friendly plastics and other materials with multiple properties.

INTRODUCTION

A sustainable society represents the ultimate goal for preserving the environment and advancing human development, and the use of environmentally friendly plastics is a necessary requirement for achieving such a society[1,2]. Plastics released into the natural environment persist for long times and affect ecosystems and human health[3-5]. Recently, segregated microplastics formed in the sea have become an issue of concern as an ocean plastic problem[6,7], and the use of biodegradable polymers represents an option for overcoming this problem [8-10]. The functional groups in a polymer dissociate during plastic degradation; however, biodegradable polymers are not typically used in everyday products, which is ascribable to issues associated with the trade-off relationship between the mechanical toughness and degradability of the polymer, where high degradability is often associated with low toughness, and vice versa.

The use of multicomponent polymers is a smart strategy for designing biodegradable polymers that are both tough and degradable. More than two monomer types that play different roles are required to produce a polymer with multiple properties. There are two components to this strategy: 1) the polymer chain structure and 2) the monomer combination. In the former case, the chain structures of several monomers are reportedly combined to produce different polymers, including polymer blends [11-13], random copolymers [14-17], di/triblock copolymers [18], and graft copolymers. The higher-order structure constructed by them strongly determines polymer properties[17,19,20]. Recently, multi-block copolymers have been investigated as biodegradable polymers[21-23]. In particular, alternating multiblock copolymers with defined block lengths and regularly repeating blocks have been shown to precisely control higher-order structures[24-27]. In the case of a crystalline polymer, multiple segments in the multiblock copolymer can generate

several higher-order structures, including segregated nanoscale crystal phases, co-crystals, amorphous miscible phases, and their mixtures. However, suitable designs of multiblock structures and the roles of higher-order structures in determining toughness and degradability are not completely clear. Indeed, evaluating all combinations of monomers in the latter case, especially those with more than two properties, is difficult, although extensive effort has been devoted to obtaining superior monomer combinations. Consequently, a methodology for effectively searching monomer combinations in terms of both toughness and degradability is highly desirable.

Machine learning techniques can be used to effectively design materials and understand their behaviour, which are often difficult for humans to recognise [28,29]. In terms of polymer design, machine learning techniques have been used to determine the optimal monomer sequences in polymers/oligomers [30-32]. For example, optimised α-amino acids in luminescent proteins have been explored using Bayesian optimisation (BO) [33]. Furthermore, optimised sequences of self-assembled peptides were explored using Monte Carlo tree-search and random-forest methods that avoid human bias [34]. It should be noted that these polymer-design targets have single properties. Recently, multi-objective optimisation, which targets multiple properties, has been applied to designing materials based on BO and generic algorithms, among others [35,36]. However, as far as we know, machine-learning-assisted designs of biodegradable polymers that are both tough and degradable has not been achieved. Machine learning techniques have also contributed to the recognition of important factors in materials, including biodegradable polymers[37-40]. Therefore, a remaining challenge involves establishing a methodology for evaluating essential multiscale and/or multimodal information factors.

Herein, we report the design, evaluation, and understanding of multiblock polyamides composed of Nylon6 and α-amino acid segments in terms of both toughness and degradability (Fig. 1). Machine-learning techniques were used to suggest optimised α-amino acid sequences in alternating multiblock copolymers that satisfy multiple properties associated with trade-off relationships. Furthermore, we revealed that multiblock structures with appropriate α-amino acid sequences and their corresponding higher-order structures significantly affect these properties.

RESULTS AND DISCUSSION

Polyamide preparation

Tough and degradable polymers were designed by selecting polyamides[25,41-46]. The amide bonds in a polyamide provide strong intermolecular interactions that engender it with toughness, high degradation selectivity, and high thermal stability; consequently, various methods for synthesising multiblock polyamides have been established [25,45]. Furthermore, a wide range of monomers, including α-amino acids, can be utilised, and monomer-sequence combinations and regularity are easily controlled. Prior to polymer synthesis, the length of the α-amino acid (αAA) sequence required for degradability was investigated using model reactions involving oligopeptides in aqueous solutions. Oligopeptides with different αAA-sequence lengths positioned between the 6-aminohexanoic acid (AHA) as monomer units of Nylon6 were enzymatically degraded using Proteinase K (Supplementary Fig. 1a). Minimal enzymatic degradation was observed for one αAA, namely Met (Supplementary Fig. 1b). The degradation rate ($\rho_{\text{enzyme, oligo}}$) of the oligopeptide was observed to increase with increasing αAA content. Three αAAs dramatically enhanced oligopeptide degradation, even at low enzyme

concentrations (Ala-Met-Ala, Supplementary Fig. 1b, oligopeptide: 1 mM, Proteinase K: 0.1 μM). Liquid chromatography–mass spectrometry (LC-MS) revealed that the C-terminus of Met is the most degraded part of the oligopeptide. On the other hand, the type of αAA sequence was also important for enhancing the oligopeptide degradation rate. For example, the degradation rate of AHA-Ala-AA^2-Ala-AHA clearly depended on the central αAA sequence (Supplementary Fig. 1c), with AHA-Ala-AA^2-Ala-AHA more suitable for enzymatic degradation than a random sequence (Supplementary Fig. 1c-d). It is worth mentioning that AHA-Ala-AHA-Ala-AHA was barely degraded under the current conditions (AHA, Supplementary Fig. 1c). We conclude that a sequence of three continuous αAAs is required for sufficient enzymatic degradation.

Polyamides were synthesised by reacting oligopeptides with coupling agents (Fig. 2a). Oligopeptides with different numbers of AHA units and fixed Ala-Met-Ala segments were reacted to determine a suitable length for the AHA segment. A peak in the higher molecular weight region was observed by gel permeation chromatography (GPC) after purification; the position of this peak effectively corresponded to that of commercially available Nylon6 (Fig. 2b). Mass spectrometry showed multiple peaks with periodic widths that correspond to dehydrated oligopeptides (Supplementary Fig. 2). These results indicate that a polyamide with an alternating multiblock structure had been successively formed. The polyamides were moulded using the solvent-casting method to prepare transparent films (Fig. 2c). Polyamide films with different numbers of AHA units were enzymatically degraded to evaluate the optimal number of AHA units. While 2AHA hardly degraded (Fig. 2d-e), the degradation rate was observed to increase as the number of AHA units was increased to four, after which it decreased (Fig. 2d-e). Polyamide films with 4AHA and 6AHA had disappeared after two days (Fig. 2d). Hence, we conclude that

4AHA has a suitable number of segments for enzymatic degradation. The mechanism responsible for these differences is discussed later. AHA and αAA sequences that are four and three units long, respectively, were used hereafter.

The degradation products of polyamide films composed of 4AHA and Ala-Met-Ala were evaluated by GPC after degradation testing with and without enzyme. The major product exhibited a slightly lower molecular weight than the original oligopeptide in the presence of the enzyme (Fig. 2f), while no corresponding peaks were observed in the absence of the enzyme. As mentioned above, amide bonds involving AHA units hardly degrade under the current conditions; therefore, the 4AHA oligopeptide was observed after the enzymatic degradation of the αAAs in the polyamide. Nylon6 itself is reportedly poorly biodegradable, whereas a Nylon6 oligomer can be metabolised in the natural environment [47]. Hence, multiblock structures offer a strategy for biodegrading Nylon6 derivatives.

Multi-objective polyamide optimisation

Prior to any multi-objective optimisation study, we investigated the material properties of polyamides with various αAA sequences. Water-soluble αAAs, such as lysine and aspartic acid, were excluded because the polyamide films were dissolved in buffer solution without enzyme. Therefore, fourteen αAAs among twenty essential ones for human were utilised, which led to $14 \times 14 \times 14 = 2744$ candidate combinations. We prepared polyamides (4AHA) with eight predetermined sequences (Ala-AA^2-Ala) and 17 random sequences (AA^1-AA^2-AA^3). Mechanical properties were evaluated by uniaxially elongating the polyamide films at room temperature. The stress–strain curve clearly depended on the αAA sequence. For example, some films were brittle like glass (blue,

Fig. 3a), while some stress–strain curve showed yield points similar to those observed for crystalline polymers (green, Fig. 3a). A small number of polyamide films exhibited elastomer-like stress–strain curves with low Young's moduli and high strains at break (orange, Fig. 3a). Polyamide films with different sequences were also subjected to enzymatic degradation, with degradation rate clearly observed to depend on the αAA sequence (Fig. 3b). Several films had almost disappeared after two days, whereas the Nylon6 film had hardly degraded under the current conditions (Supplementary Fig. 3a). Other representative biodegradable polymers, such as polylactic acid (PLLA), polybutylene succinate (PBS), and polybutylene succinate-co-adipate (PBSA), were also less degradable (Supplementary Fig. 3a). The polyamide films did not always show degradation behaviour consistent with that of the oligopeptides (Fig. 6a), which will be discussed later. These results reveal that the αAA sequence significantly affects the toughness and enzymatic degradability of a polyamide film.

We next subjected the AA sequence in the polyamide to multi-objective optimisation for toughness and degradability. T-scales were used as αAA descriptors [48]. Bayesian optimisation (BO) based on Gaussian process regression was used, where the expected hypervolume improvement (EHVI) and Thompson sampling (TS) were the objective functions of the multi-objective BO. We first attempted to optimise the enzymatic degradation rate and strain at break, which revealed trade-off relationships in all but one sample (Fig. 4a-b). The EHVI exhibited a remarkable improvement in the Pareto solution (ochre, Fig. 4b); therefore, we used multi-objective optimisation in the current approach. However, this sample exhibited elastomer-like stress–strain curves with a low Young's modulus (ochre, Fig. 4d). Therefore, we performed a multi-objective optimisation for three objects (degradation rate, strain at break, and Young's modulus).

The Gly-Leu-Ala-containing polyamide exhibited Pareto regions in two scatter plots (purple, Fig. 4b-c), as suggested by EHVI. Furthermore, the stress–strain curve of the polyamide revealed behaviour similar to that of a crystalline polymer. The strain at break of the polyamide was determined to be higher than that of Nylon6 prepared by solvent casting, but lower than that of Nylon6 moulded by hot pressing (Supplementary Fig. 3b). Films with the suggested αAA sequences showed low enzymatic degradation rates for both two and three objects when TS was used as the objective function. Nevertheless, polyamides with superior enzymatic degradabilities and high mechanical performance were obtained via BO-based multi-objective optimisation.

Phase separation in a multiblock polyamide

A multiblock polyamide is expected to form an aggregated structure on the nanoscale because AHA and αAA segments are repeatedly located in one chain. Therefore, the thermal properties and nanoscale structures of the polyamides were evaluated using differential scanning calorimetry (DSC), wide-angle X-ray scattering (WAXS), and small-angle X-ray scattering (SAXS) experiments. The DSC curve of the Gly-Leu-Ala-containing polyamide exhibited a baseline shift at 50 °C during first heating, which is close to the glass transition temperature (T_g) of Nylon6 (Supplementary Fig. 3c). Two overlapping melting peaks were observed at 190 °C; these peaks were separately observed at 190 and 240 °C in the case of Ala-Met-Ala (blue, Fig. 6c). The melting point of poly(αAA) is reportedly higher than that of Nylon6 [49]; hence, the two melting peaks are derived from the AHA-rich and αAA-rich phases. Diffraction peaks at q ~14 nm^{-1} and an amorphous halo, whose ratios depended on the αAA sequence, were observed by WAXS (Fig. 5a), while SAXS revealed a scattering peak at q ~1.2 nm^{-1} for the Ala-Leu-

Ala-containing polyamide, which is higher than that of a long-range structure that corresponds to the lamella thickness of Nylon6 (Fig. 5b). This peak was less intense for some samples (e.g., Gly-Leu-Ala, red, Fig. 5b). Furthermore, the Ala-Met-Ala film was transparent, and no structures were observed by polarisation microscopy (Fig. 2c). These results show that these multiblock copolymers form phase-separated structures composed of AHA and αAA segments on the several-nanometre scale without the formation of spherulites, and that the clarity of the structure depends on the sequences.

The phase-separated structure was altered by heating, as evidenced by changes in the DSC curves observed during the second heating process, in which T_g peaks became more intense and melting peaks disappeared (Supplementary Fig. 3c). WAXS and IR techniques were used to confirm heating-related changes in crystal structure. A diffraction peak was observed for Ala-Met-Ala to 210 °C; this peak disappeared with further heating above 250 °C, which is above the second melting peak in the DSC curve (Supplementary Fig. 4a and Fig. 6c), indicating that the diffraction peaks at q ~14 nm^{-1} are derived from the crystal structures of αAA-rich phases [42]. Hence, αAA-rich phases crystallise in the phase-separated polyamide films. The crystal peaks in the WAXS profiles were not regenerated by maintaining the film at 140 °C for 10 min after being heating above their melting points (T_m), which is consistent with the absence of any melting peak during the second DSC heating process (Supplementary Fig. 3c and Fig. 5c). Furthermore, the two overlapping peaks that correspond to the stretching vibrations of hydrogen-bonded C=O groups in the AHA-rich and αAA-rich phases were observed as a single peak in the IR spectrum after the polyamide films had been heated above T_m (Fig. 5d and Supplementary Fig. 4b). In terms of T_g, the baseline for the Gly-Leu-Ala-containing polyamide appeared to shift at ~80 °C, which is between the T_g regions of the AHA-rich and αAA-rich phases

(green, Supplementary Fig. 3c). Hence, the phase-separated structure disappeared when heated above the melting point of the αAA-rich phases to form a non-crystalline miscible system. We conclude that a phase-separated structure was formed during the solvent-casting process given that the two segments are miscible when heated [50].

Effect of the higher-order structure on properties

We speculated that both the αAA sequence and the higher-order structure of a polyamide contribute to both of the abovementioned properties, as heating a polyamide film above its melting point alters its phase-separated and crystal structure. Therefore, we subjected films thermally treated at 100 and 220 °C, which are below and above their melting points, respectively, to tensile testing. The polyamide films treated at 100 °C still showed yield points in their stress–strain curves when heated, although less stress was observed (Fig. 5e). The mechanical properties of the polyamide were sufficiently maintained because the crystal structure is maintained up to the melting point. Nylon6 also exhibited lower stress, whereas the range of decrease was less, probably because it is more crystalline than the polyamide (Supplementary Fig. 5a-b). On the other hand, the polyamide films treated at 220 °C (which are not crystalline) are brittle at room temperature and become quite soft when heated (Fig. 5f). Because the thermally treated films have glass transition temperatures of about 80 °C, they transform from their glass states to melt/rubber states when heated during tensile testing. Hence, a phase-separated crystal structure endows the multiblock polyamide with high mechanical performance, especially when heated.

As mentioned in the previous section, the enzymatic degradabilities of polyamides with different numbers of AHA units and fixed Ala-Met-Ala sequences reveal

that 4AHA is optimal (Fig. 2e). This tendency runs contrary to the expectation that a low AHA ratio affords a high degradation rate owing to the high volume fraction of αAA segments during enzyme dissociation. Therefore, we investigated the effect of higher-order structures on degradability. The intensity of the hydrogen-bonded C=O peak (1621 cm^{-1}) in the IR spectrum was observed to decrease as the number of AHA units was increased, while the peak corresponding to Nylon6 became less intense (Supplementary Fig. 6a); furthermore, the WAXS diffraction peaks at q ~14 nm^{-1} also became less intense (Supplementary Fig. 6b). DSC revealed that the melting points of the αAA-rich phases (220–270 °C) decreased as the number of AHA units was increased, despite the AHA-rich phase maintaining a melting point of ~190 °C (Supplementary Fig. 6c). These observations suggest that an increase in the volume fraction of AHA segments reduces the crystal size or order of the αAA-rich phases. It is well known that enzymes preferentially degrade amorphous regions of crystalline polymers. In other words, the multiblock structure destroys the crystal structures of the αAA segments and enhances enzymatic degradation. These decreases in the volume fraction and crystal order of the αAA-rich phases contribute the reversing degradability trend observed; hence, the 4AHA-containing polyamide showed maximum enzymatic degradation.

The enzymatic degradation ratios of some films deviated from those of the oligopeptides, which indicates that other factors also influence degradability (Fig. 6a). For instance, oligopeptide samples that degraded poorly in solution were highly degradable in the film state. These differences are attributable to the presence of surfaces or different higher-order structures in the film states. These differences were investigated by extracting more than 40 physical values from a number of experimental and quantum-chemical studies (Fig. 6b-e, Supplementary Fig. 7a). For example, the widths of the

WAXS diffraction peaks (σ_{WAXS}) were used as indicators of the crystal sizes of the αAA segments. The affinities of the αAA segments for water were calculated based on quantum-chemically calculated hydration energies ($\Delta E_{hydration}$). How these factors impact film degradability ($\rho_{enzyme,\ film}$) was evaluated based on ridge regression, LASSO regression, and multiple linear regression with sequential feature selectors (Fig. 6f, Supplementary Fig. 7b-c), with mean-squared errors of 0.135, 0.202, and 0.292 determined, respectively, for the test data; consequently, we discuss the ridge regression analysis results. In addition to oligopeptide degradability, several other factors were identified as important features (Fig. 6f). For example, σ_{WAXS1} and μ_{WAXS1} were found to positively correlate with $\rho_{enzyme,\ film}$, which shows that polyamide films with smaller or more disordered αAA-rich-phase crystals are more degradable. The melting temperatures of the AHA-rich phases ($T_{m,AHA}$) were found to correlate negatively with $\rho_{enzyme,\ film}$, which indicates that segment disorder increases degradability. The relative area of peak7 in the IR spectrum ($Area_{IR7}$) was found to positively correlate with $\rho_{enzyme,\ film}$, which reveals that more free C=O bonds or miscible phases enhance degradability. Furthermore, hydration energy ($\Delta E_{hydration}$) negatively affects $\rho_{enzyme,\ film}$, suggesting that the strong affinity of polyamide for water enhances degradability. Consequently, we revealed that, in addition to the degradability of the αAA sequence itself, chain properties (e.g., hydrophilicity) and higher structures (e.g., crystal structures) significantly affect enzymatic degradability.

Polyamide degradation in the natural environment

Although degradation experiments using enzymes were carried out in vitro, degrading polyamides in the natural environment is desirable. Therefore, polyamides were degraded in muddy water; here, polyamide films were immersed at room

temperature in ten-fold concentrated muddy water collected from paddy fields around Kyushu University. Several samples were confirmed to have lost wight after five days, although Nylon6 was hardly degraded (Supplementary Fig. 8a-b). Notably, the Gly-Leu-Ala-containing polyamide, which exhibited high mechanical performance (as discussed above) was one of the degraded samples (Fig. 4), from which we conclude that the current polyamide design usefully promoted degradation in the natural environment. Degradation under other natural conditions and the associated degradation mechanism will be addressed in future work.

CONCLUSION

We demonstrated tough and degradable multiblock polyamides that were designed using machine learning techniques. Alternating multiblock copolymers composed of Nylon6 and α-amino acid segments were prepared by coupling oligopeptides. A sequence of three continuous α-amino acids was found to endow the polymer with versatile material properties and enhanced enzymatic degradability. Multi-objective optimisation based on BO suggested appropriate α-amino acid sequences that were both mechanical tough and degradable. The higher-order structure generated by the multiblock assembly was important for achieving this outcome, with machine learning techniques revealing essential factors among experimental and calculational data. In addition, some materials exhibited degradability in the natural environment or muddy water.

Key points to consider when breaking down the trade-off relationship observed for the biodegradable polymers in this study include adaptation of the multiblock structure and the utilisation of machine learning techniques. The Nylon6 (AHA) and α-amino acid

segments in the multiblock copolymers play different roles in determining toughness and degradability. The phase-separated two-segment structure enables the formation of a moderate nanometre-scale crystal structure, which endows toughness even when heated owing to the high melting temperatures of these materials. In addition, smaller αAA-rich-phase crystals or a lower crystal order associated with the inclusion of AHA segments enhances enzymatic degradability. It is worth mentioning that the Nylon6 oligomer generated by degradation can be metabolised in the natural environment. On the other hand, machine learning techniques contributed to the design of the monomer sequence and mechanistic understanding. Generally, humans struggle to predict the material properties of the many possible three-amino-acid sequences, especially multiple properties, and identifying the essential factors of higher-order structures using multimodal experimental and simulation data is also difficult. Our approach, which uses multiblock copolymers and machine learning techniques, is a useful method for designing and understanding environmentally friendly plastics and other materials that require multiple properties.

Acknowledgements

The synchrotron radiation experiments were performed at the BL40XU and BL05XU beamlines of SPring-8 with the approval of the Japan Synchrotron Radiation Research Institute (JASRI) (Proposal No. 2020A1525, 2021B1476 and 2022B1029). This work was supported by the Cabinet Office, Government of Japan, Cross-ministerial Strategic Innovation Promotion Program (SIP), “Technologies for Smart Bio-industry and Agriculture” (funding agency: Bio-oriented Technology Research Advancement Institution, NARO). This paper is based on results obtained from a project, JPNP18016,

commissioned by the New Energy and Industrial Technology Development Organization (NEDO). This work was also supported by the JSPS Grant-in-Aid for Scientific Research on Innovative Areas, Discrete Geometric Analysis for Materials Design: 20H04644, by the Grant-in-Aid for Scientific Research (B): 20H02800 and Data Creation and Utilization Type Material Research and Development Project Grant Number JPMXP1122683430. Y.A. and K.T. acknowledges the financial support of the Grant-in-Aid for RIKEN-Kyushu Univ Science and Technology Hub Collaborative Research Program.

METHODS

Materials

Fmoc-αAA-OH, *N*-Hydroxysuccinimide (NHS), 1-(3-dimethylaminopropyl)-3-ethylcarbodiimide hydrochloride (EDC·HCl), 6-aminohexanoic acids (AHA), 1-hydroxybenzotriazole (HOBt), diisopropylcarbodiimide (DIC), piperidine, 3-[bis(dimethylamino)methyliumyl]-3H-benzotriazol-1-oxide hexafluorophosphate (HBTU), and dimethyl formamide (DMF) were purchased from Watanabe Chem. Ind., LTD. Trifluoro acetic acid (TFA), diisopropyl ethyl amine (DIEA), 2,2,2-trifluoroethanol (TFEt), and tetraethylene glycol monomethyl ether (TEG) were obtained from Tokyo Chemical Industry Co., Ltd. Triisopropyl silane (TIPS) was purchased from FUJIFILM Wako Pure Chemical Corporation. 2-Chlorotrityl chloride resin was obtained from GL Biochem Ltd. Nylon6 was purchased from Sigma-Aldrich Co. LLC. Fmoc-AHA-OH was synthesized by a coupling reaction of Fmoc-OSu and AHA as previously reported [51].

Synthesis of Fmoc-AHA-AHA-OH

Fmoc-AHA-OH (43.8 g, 124 mmol), NHS (21.4 g, 186 mmol) and chloroform (620 mL) were poured into in 1 L round-bottom flask after which EDC·HCl (35.7 g, 186 mmol) was added portion wise over 5 min. The mixture was stirred at room temperature for 3 h, washed twice with water (270 mL) containing brine (30 mL), and three times with aqueous 0.1 N HCl (270 mL) containing brine (30 mL). The organic layer was dried using magnesium sulfate for 30 min, filtered, and the filtrate was evaporated and dried under vacuum. AHA (17.9 g, 136 mmol), water (300 mL), acetone (300 mL), and sodium hydrogen carbonate (20.8 g, 248 mmol) were then added and the mixture was stirred at room temperature for 20 h. The acetone was removed by evaporation, and chloroform

(300 mL) and 2 N aqueous HCl (170 mL) were added to neutralise the solution, which was then extracted twice with chloroform (2 × 150 mL). The combined organic layers were dried using magnesium sulfate, after which the residue was dissolved in hexane (300 mL) and the solution was stored in a freezer for 20 h. The solid was collected by filtration and dried under vacuum. This precipitation process was repeated three times to afford the product as a white powder (44.7 g, 95.8 mmol (77% yield)). ^{1}H-NMR (DMSO-d6): δ/ppm 1.25 (m, 4H, CH_2), 1.38 (m, 4H, CH_2), 1.49 (m, 4H, CH2), 2.03 (t, J = 7 Hz, 2H, CH_2), 2.19 (t, J = 7 Hz, 2H, CH_2), 3.00 (m, 4H, CH2), 4.21 (t, J = 7 Hz, 1H, CH), 4.29 (d, J = 7 Hz, 2H, CH2), 7.33-7.90 (m, 8H, aromatic). ^{13}C-NMR (DMSO-d6): δ 24.7, 25.5, 26.4, 26.5, 29.4, 29.6, 34.1, 35.9, 38.7, 47.3, 65.6, 120.5, 125.6, 127.5, 128.0, 141.2, 144.4, 156.5, 172.3, 174.9. HRMS exact mass calculated for $[M+1]^+$ $C_{27}H_{35}N_2O_5$ 467.2540, found 467.2546.

Synthesis of Fmoc-AHA-AHA-AHA-OH

Fmoc-AHA-AHA-AHA-OH was synthesised in the same manner as Fmoc-AHA-AHA-OH using Fmoc-AHA-AHA-OH (21.0 g, 45.0 mmol), NHS (7.77 g, 67.5 mmol), EDC·HCl (12.9 g, 67.5 mmol), AHA (6.49 g, 49.5 mmol), and sodium hydrogen carbonate (7.56 g, 90 mmol). The product was obtained as a white powder (22.2 g, 38.2 mmol (85% yield)). ^{1}H-NMR (DMSO-d6): δ/ppm 1.22 (m, 6H, CH_2), 1.37 (m, 6H, CH_2), 1.47 (m, 6H, CH_2), 2.03 (t, J = 7 Hz, 4H, CH_2), 2.19 (t, J = 7 Hz, 2H, CH_2), 3.00 (m, 6H, CH_2), 4.21 (t, J = 6 Hz, 1H, CH), 4.29 (d, J = 6 Hz, 2H, CH_2), 7.31-7.90 (m, 8H, aromatic). ^{13}C-NMR (DMSO-d6): δ 24.7, 25.5, 26.4, 26.6, 29.4, 29.6, 34.1, 35.9, 38.7, 38.8, 39.4, 47.3, 65.6, 120.5, 125.6, 127.5, 128.0, 141.2, 144.4, 156.5, 172.3, 174.9. HRMS exact mass calculated for $[M+1]^+$ $C_{33}H_{46}N_3O_6$: 580.3381, found: 580.3387.

Synthesis of Fmoc-AHA-AHA-AHA-AHA-OH

Fmoc-AHA-AHA-AHA-AHA-OH was synthesised in the same manner as Fmoc-AHA-AHA-OH using Fmoc-AHA-AHA-AHA-OH (11.6 g, 20.0 mmol), NHS (3.45 g, 30.0 mmol), EDC·HCl (5.75 g, 30.0 mmol), AHA (2.89 g, 22.0 mmol), and sodium hydrogen carbonate (3.36 g, 40.0 mmol). The product was obtained as a white powder (11.3 g, 16.3 mmol (82% yield)). ^{1}H-NMR (DMSO-d6): δ/ppm 1.22 (m, 8H, CH_2), 1.37 (m, 8H, CH_2), 1.47 (m, 8H, CH_2), 2.03 (t, J = 7 Hz, 6H, CH_2), 2.19 (t, J = 7 Hz, 2H, CH_2), 3.00 (m, 8H, CH_2), 4.21 (t, J = 6 Hz, 1H, CH), 4.29 (d, J = 6 Hz, 2H, CH_2), 7.31-7.90 (m, 8H, aromatic). ^{13}C-NMR (DMSO-d6): δ 24.7, 25.5, 26.4, 26.6, 29.4, 29.6, 34.1, 35.9, 38.7, 38.8, 47.3, 65.6, 120.5, 125.6, 127.5, 128.0, 141.2, 144.4, 156.5, 172.3, 174.8. HRMS exact mass calculated for $[M+1]^+$ $C_{39}H_{57}N_4O_7$: 693.4222, found: 693.4227.

Preparing oligopeptides

Oligopeptides composed of AHA and α-amino acids were prepared by solid-phase peptide synthesis. In a typical run, Fmoc-AHA-AHA-OH (303 mg, 649 μmol) was coupled to 2-chlorotrityl chloride resin (500 mg, loading: 1.18 mmol/g) using dichloromethane (9 mL) and DIEA (200 mL, 1.15 mmol) in a reaction tube. After stirring for 40 min at room temperature, the resin was washed three times with dichloromethane containing DIEA (2.5% v/v) and methanol (2.5% v/v) and three times with DMF. The Fmoc group was deprotected by treatment with a mixture of DMF and piperidine (80/20 (v/v)) twice. After 10 min, the resin was washed seven times with DMF. Fmoc-Ala-OH (606 mg, 1.94 mmol) was coupled with DIC (302 μL, 1.95 mmol) and HOBt (298 mg, 1.95 mmol) in DMF for 2 h at room temperature. The resin was washed seven times with

DMF. This coupling cycle was repeated using Fmoc-Phe-OH (754 mg, 1.95 mmol) and Fmoc-Ala-OH (606 mg, 1.95 mmol), after which Fmoc-AHA-AHA-OH (908 mg, 1.95 mmol) was coupled with HBTU (671 mg, 1.77 mmol) and DIEA (514 μL, 2.95 mmol) at room temperature for 2.5 h. After washing and deprotection, the resin was treated with methanol three times and dried under vacuum. The resin was removed using TFA (400 μL) and TIPS (0.6 mL) in dichloromethane (12 mL) at room temperature for 40 min. The reaction mixture was filtered, evaporated, and precipitated with DMF (5 mL) in chloroform and hexane (1/2 (v/v)). The product (H_2N-AHA-AHA-Ala-Phe-Ala-AHA-AHA-OH·TFA) was obtained as white powder (396 mg, 453 μmol, 70% yield). ^{1}H-NMR (DMSO-d6): δ/ppm 1.11-1.55 (m, 24H, CH_2), 2.01-2.09 (m, 6H, CH_2), 2.18 (t, J = 7H, CH_2), 2.74-2.78 (m, 2H, CH_2), 2.79-2.85 (m, 1H, CH_2), 2.98-3.06 (m, 7H, CH_2), 4.19 (q, *J* = 7Hz, 2H, CH), 4.46 (m, 1H, CH), 7.16-7.26 (m, 5H, aromatic), 7.68-7.97 (m, 6H, NH). MALDI-TOF-MS analysis calculated for $[M+1]^+$ $C_{39}H_{66}N_7O_8$: 761.0, found: 760.5.

Polyamide synthesis

In a typical run, HOBt (175 mg, 1.14 mmol), DIC (179 μL, 1.15 mmol), and DIEA (331 mL, 1.90 mmol) were added to H_2N-AHA-AHA-Ala-Phe-Ala-AHA-AHA-OH·TFA (332 mg, 0.38 mmol) in DMSO (1.21 mL) at room temperature. After 1 h, the reaction mixture was heated to 60 °C and maintained at this temperature for 2 d. The solid was dissolved in TFEt (4 mL) and precipitated twice from a mixture of chloroform and hexane (4/1 v/v)). The polyamide was treated with TFA, TIPS, and water (= 95/2.5/2.5 v/v/v) for 2 h when amino acids with protected side-chain were involved, and precipitated in a mixture of diethyl ether and hexane (= 9/1 (v/v). The product was obtained as a white powder (154 mg, 47% yield). GPC (TFEt with sodium trifluoroacetate (5 mM)): M_n =

4800, M_w/M_n = 5.3. MALD-TOF-MS analysis calculated for [3M (cyclic)+Na]$^+$ $C_{117}H_{189}N_{21}NaO_{21}$: 2247.5, found: 2249.1.

Film moulding

The polyamide was moulded by solvent casting, while Nylon6 was moulded by solvent casting and hot pressing. Polyamide or Nylon6 (180 mg) was dissolved in TFEt (3.4 mL) and poured into a PTFE mould (4.5 cm × 3.5 cm) and kept horizontal overnight. The dried sample was heated at 80 °C for 3 h and at 100 °C for 2 h under vacuum, to afford an approximately 100-μm-thick polyamide film. In the case of hot pressing, Nylon6 was melted at 240 °C in a hot-press machine under vacuum for 10 min at 10 MPa using a silicon wafer modified with *n*-octadecyltrimethoxysilane. The sample was then crystallised in another hot-press machine at 142 °C for 20 min at 5 MPa. Melted samples were treated in ice water without crystallisation to produce quenched samples.

Tensile testing

Tensile testing was performed by uniaxially elongating polyamide films. Samples were cut using a 2 × 12 mm dumbbell-shaped mould. Uniaxial elongation was carried out using a tensile-testing machine (Imoto Machinery CO., Ltd.) at 10 mm/min and room temperature or 100 °C. Young's moduli were calculated based on the initial slopes of the stress–strain curves. Strains at break were evaluated as the strains at which samples separated. Both values are reported as the averages of three tests.

Enzymatically degrading oligopeptides

Oligopeptides (AHA-AA^1-AA^2-AA^3-AHA) were prepared as described above. The N-terminus of each peptide consisted of an amino group for sequences with AA^1 and

AA^3 = Ala, and an acetyl group for random sequences. The C-terminus was modified with an amide group using a rink-amide resin. In a typical run, Proteinase K (0.1 μM) with TEG (100 μM) as an internal standard, and an oligopeptide (1 mM) were added to a Tris-buffered saline solution and allowed to react in a heated bath at 37 °C. After 30 min, the reaction solution was diluted 10-times with water containing formic acid (0.1%, v/v) and allowed to deactivate at 98 °C for 15 min. The amount of oligopeptide was determined by liquid chromatography–mass spectrometry using an LCMS-2020 and Nexera X2 system (Shimadzu Corp.). The eluent, which consisted of aqueous formic acid and methanol (98/2 to 0/100 (v/v)), was flowed at 1.5 mL/min. The reaction mixture was separated using an ODS column (TSKgel ODS120-H (TOSOH Corp.)) at 40 °C. Compounds were ionised using the ESI method and detected using a quadrupole mass spectrometer in positive mode. The areas of the peaks in the mass spectra of the oligopeptides before and after reaction (A_{before} and A_{after}) were standardised against those of TEG. The enzymatic degradation rate was calculated as $\rho_{\text{enzyme, oligo}} = 1 - A_{\text{after}}/A_{\text{before}}$ using the average values from three runs.

Enzymatically degrading polyamides

Polyamides were enzymatically degraded by immersing films in Proteinase K solution. Polyamide films (~100-μm thick) were cut to rectangular shapes that were approximately 5 mg in weight. Each film was immersed in a solution of Proteinase K in Tris-buffered saline (0.5 mg/mL, 0.8 mL, pH 7.4) for 2 d at 37 °C. The ratio of the film remaining following enzyme treatment (r_{enzyme}) was calculated from the weights of the film before and after degradation ($w_{\text{before, enzyme}}$ and $w_{\text{after, enzyme}}$, respectively) as: $r_{\text{enzyme}} = w_{\text{after, enzyme}}/w_{\text{before, enzyme}}$. Films were concurrently treated with Tris buffer devoid of

enzyme as a control, and the remaining ratio in the absence of enzyme (r_{buffer}) was evaluated as described above. The enzymatic degradation rate was calculated as: $\rho_{enzyme,\ film} = 1 - r_{enzyme}/r_{buffer}$ using the average values from three experiments.

Degrading polyamides in muddy water

Polyamides were degraded under natural conditions by immersing films in muddy water. Polyamide films (~100-μm thick) were cut into rectangular shapes approximately 1.5 mg in weight. Muddy water was collected from a paddy field around Kyushu University, sonicated for 10 s, and concentrated 10 times under vacuum. Films were immersed in the concentrated muddy water (1 mL) at room temperature for 5 d. The ratio of each film remaining in the muddy water (r_{muddy}) was determined by weighting the film before and after degradation ($w_{before,\ muddy}$ and $w_{after,\ muddy}$, respectively) as: $r_{muddy} = w_{after,\ muddy}/w_{before,\ muddy}$. Films were also concurrently treated in muddy water deactivated by heating at 98 °C for 10 min as a control, and the remaining ratio ($r_{control}$) was evaluated using the same equation. The degradation rate of the polyamide in muddy water was calculated as: $\rho_{muddy,\ poly} = 1 - r_{muddy}/r_{control}$. Average values and standard deviations determined from four of five test samples were used, with one outlier excluded.

WAXS/SAXS experiments

WAXS and SAXS experiments were performed on the BL05XU beamline of the SPring-8 facility. Each film was exposed to X-rays with a wavelength of 0.1 nm for 1 s at room temperature, and detected using SOPHIAS and PILATUS detectors with sample-to-detector distances of 159 and 1378 mm for WAXS and SAXS, respectively. The sample-to-detector distance and beam centre were determined using CeO_2 and AgBe as

WAXS and SAXS standards, respectively. Two-dimensional images were converted into one-dimensional profiles using FIT2D software. Profiles were subtracted from background samples without the use of any coefficients. The scattering vector is defined as: $q = 4\pi \sin\theta/\lambda$, where λ is the X-ray wavelength, and 2θ is the scattering angle.

Differential scanning calorimetry

DSC was performed using a NEXTA DSC200 instrument (Hitachi High-Tech Corp.) in temperature-modulated mode. Each film (~ 3 mg) was placed in an aluminium pan and sealed, and a film-free aluminium pan was prepared as a reference sample. The samples were cooled to −40 °C at 10 °C/min, and then heated to 240 °C at 2 °C/min with a temperature amplitude of 0.5 °C and a frequency of 0.012 Hz. This protocol was repeated under the same conditions for a second cycle. The acquired curves (total) were separated into reversing and non-reversing components using NEXTA software, and the reverse components were plotted in this study.

Gel permeation chromatography

GPC was conducted using a Prominence HPLC system (Shimadzu Corp.) equipped with LC-20AD, CTO-20AC, SPD-20A, and RID-10A components. Sodium trifluoroacetate (5 mM) in TFEt was used as the eluent at 3 mL/min. The polyamide was dissolved in TFEt (5 mg/mL, 20 μL) and injected onto and separated by TSKgel SuperAW4000 and SuperAW3000 columns at 40 °C, and detected by an RI detector. Five polystyrene standard samples (M_p = 1.1 × 10^5, 5.3 × 10^4, 2.1 × 10^4, 4.9 × 10^3, and 1.9 × 10^3) were used to construct the calibration curve from which M_n and M_w/M_n values were evaluated.

IR spectroscopy

Fourier-transform infrared (FT-IR) spectroscopy was carried out using an INVENIO X (Bruker) spectrometer in attenuated total reflection mode. Each polyamide film was placed in the Gladi ATR unit (PIKE Tech.) and fixed using a pin. Spectra were acquired at room temperature in the 4000–500 cm^{-1} wavenumber range with a resolution of 2 cm^{-1} and sixteen scans. IR spectra were obtained by subtracting the sample-free background spectra.

Quantum chemical calculations

Oligopeptides with Ac-AHA-AA^1-AA^2-AA^3-AHA-NH_2 sequences were subjected to quantum-chemical calculations using Gaussian 16 software. We first used Balloon [52], a conformer-searching tool implemented in Winmostar [53] that uses a multi-objective genetic algorithm, to search for stable oligopeptide conformations using the MMFF94 force field [52]. Structures were optimised at the B3LYP/6-31G** level [54-57] in Gaussian 16 [58]. The effect of water as the solvent was included using the polarisable continuum model (ε = 78.3553) [59]. The hydration energy of each polyamide ($\Delta E_{hydration}$) was obtained as the difference between the energies in water (E_{water}) and in a vacuum (E_{vacuum}).

Multi-objective optimisation using BO

Multiple properties were subjected to Bayesian optimisations using Gaussian process regression (GPR) in PHYSBO software [60]. The T-scale was adopted as the α-amino acid descriptor [48], in which the T1, T2, and T3 values of the three α-amino acids

(a total of nine values) were used as explanatory variables. Young' modulus, strain at break, and the enzymatic degradability of each polyamide film thermally treated at 80 °C were utilised as objective variants. Eight Ala-AA^2-Ala samples and 17 samples of random sequences (AA^1-AA^2-AA^3) were used to construct GPR models. Multi-objective optimisations were performed using hypervolume-based probability of improvement (HVPI) [61], EHVI[61], and TS[62] as objective functions. The suggested sequence of three α-amino acids was obtained by excluding of water-soluble ones from 14 (AA^1) × 14 (AA^2) × 14 (AA^3) – 25 (original) = 2719 combinations, which were synthesised and re-evaluated. In the current study, the sequences suggested by HVPI and EHVI were the same in most cases.

Evaluating important physical values

Important physical values for enzymatic degradability were evaluated by ridge regression[63], LASSO regression[64], and linear regression with sequential feature selectors (SFS) [65] using the scikit-learn library. Information, such as T_g, T_m, ΔH_{melt}, peak position/width/relative area after peak fitting, and film crystallinity were extracted from DSC, WAXS, and IR data. The hydrophilicities of the αAA sequences were evaluated using quantum-chemical calculations. Consequently, more than 40 values were extracted as explanatory variables. Nested leave-one-out cross-validation (LOOCV) was adopted, in which one test sample was eliminated to evaluate the mean-squared error, while the others were used to determine regularity parameters and coefficients; this treatment was repeated by changing the test sample. Therefore, many more coefficients than the sample size (26) were calculated. New explanatory variables were sequentially added using improved ones (compared with other explanatory variables) based on the mean squared

error (MSE) of the validation data when the SFS linear regression method was used. Explanatory variables were then added until the MSE improved. The important feature values for each combination were evaluated using the average values of the regression coefficients of the various models.

References

1 Manker, L. P. *et al.* Sustainable polyesters via direct functionalization of lignocellulosic sugars. *Nat Chem* **14**, 976–984, doi:10.1038/s41557-022-00974-5 (2022).

2 Li, X. L., Clarke, R. W., Jiang, J. Y., Xu, T. Q. & Chen, E. Y. X. A circular polyester platform based on simple gem-disubstituted valerolactones. *Nat Chem* **15**, 278–285, doi:10.1038/s41557-022-01077-x (2023).

3 Gross, R. A. & Kalra, B. Biodegradable polymers for the environment. *Science* **297**, 803–807, doi:10.1126/science.297.5582.803 (2002).

4 Haider, T. P., Volker, C., Kramm, J., Landfester, K. & Wurm, F. R. Plastics of the Future? The Impact of Biodegradable Polymers on the Environment and on Society. *Angew Chem Int Edit* **58**, 50–62, doi:10.1002/anie.201805766 (2019).

5 Fagnani, D. E. *et al.* 100th Anniversary of Macromolecular Science Viewpoint: Redefining Sustainable Polymers. *ACS Macro Lett* **10**, 41–53, doi:10.1021/acsmacrolett.0c00789 (2021).

6 Isobe, A., Iwasaki, S., Uchida, K. & Tokai, T. Abundance of non-conservative microplastics in the upper ocean from 1957 to 2066. *Nat Commun* **10**, 417, doi: 10.1038/s41467-019-08316-9 (2019).

7 Shruti, V. C. & Kutralam-Muniasamy, G. Bioplastics: Missing link in the era of Microplastics. *Sci Total Environ* **697**, 134139, doi: 10.1016/j.scitotenv.2019.134139 (2019).

8 Nair, L. S. & Laurencin, C. T. Biodegradable polymers as biomaterials. *Prog Polym Sci* **32**, 762–798, doi:10.1016/j.progpolymsci.2007.05.017 (2007).

9 Tokiwa, Y., Calabia, B. P., Ugwu, C. U. & Aiba, S. Biodegradability of Plastics. *Int J Mol Sci* **10**, 3722–3742, doi:10.3390/ijms10093722 (2009).

10 Delre, C. *et al.* Near-complete depolymerization of polyesters with nano-dispersed enzymes. *Nature* **592**, 558–563, doi:10.1038/s41586-021-03408-3 (2021).

11 Abe, H., Matsubara, I. & Doi, Y. Physical-Properties and Enzymatic Degradability of Polymer Blends of Bacterial Poly[(R)-3-Hydroxybutyrate] and Poly[(R,S)-3-Hydroxybutyrate] Stereoisomers. *Macromolecules* **28**, 844–853, doi:10.1021/ma00108a007 (1995).

12 Mathew, A. P., Oksman, K. & Sain, M. Mechanical properties of biodegradable composites from poly lactic acid (PLA) and microcrystalline cellulose (MCC). *J Appl Polym Sci* **97**, 2014–2025, doi:10.1002/app.21779 (2005).

13 Jiang, L., Wolcott, M. P. & Zhang, J. W. Study of biodegradable polyactide/poly(butylene adipate-co-terephthalate) blends. *Biomacromolecules* **7**, 199–207, doi:10.1021/bm050581q (2006).

14 Xu, J. & Guo, B. H. Poly(butylene succinate) and its copolymers: Research, development and industrialization. *Biotechnol J* **5**, 1149–1163, doi:10.1002/biot.201000136 (2010).

15 Zhou, J. B. *et al.* Biodegradable poly(amine-co-ester) terpolymers for targeted gene delivery. *Nat Mater* **11**, 82–90, doi:10.1038/Nmat3187 (2012).

16 Oniki, Y. *et al.* Molecular design of environmentally benign segmented polyurethane(urea)s: effect of the hard segment component on the molecular aggregation states and biodegradation behavior. *Polym Chem* **4**, 3735–3743, doi:10.1039/c3py00172e (2013).

17 Arandia, I. *et al.* How Composition Determines the Properties of Isodimorphic Poly(butylene succinate-ran-butylene azelate) Random Biobased Copolymers: From Single to Double Crystalline Random Copolymers. *Macromolecules* **48**, 43–57, doi:10.1021/ma5023567 (2015).

18 Jeong, B., Bae, Y. H., Lee, D. S. & Kim, S. W. Biodegradable block copolymers as injectable drug-delivery systems. *Nature* **388**, 860–862, doi:Doi 10.1038/42218 (1997).

19 Castillo, R. V. & Muller, A. J. Crystallization and morphology of biodegradable or biostable single and double crystalline block copolymers. *Prog Polym Sci* **34**, 516–560, doi:10.1016/j.progpolymsci.2009.03.002 (2009).

20 Zheng, Y. & Pan, P. J. Crystallization of biodegradable and biobased polyesters: Polymorphism, cocrystallization, and structure-property relationship. *Prog Polym Sci* **109**, 101291, doi: 10.1016/j.progpolymsci.2020.101291 (2020).

21 Jeon, O., Lee, S. H., Kim, S. H., Lee, Y. M. & Kim, Y. H. Synthesis and characterization of poly(L-lactide)-poly(epsilon-caprolactone) multiblock copolymers. *Macromolecules* **36**, 5585–5592, doi:10.1021/ma034006v (2003).

22 Cakir, S., Kierkels, R. & Koning, C. Polyamide 6-Polycaprolactone Multiblock Copolymers: Synthesis, Characterization, and Degradation. *J Polym Sci Pol Chem* **49**, 2823–2833, doi:10.1002/pola.24716 (2011).

23 Liu, S. Y., Li, C. G., Zhao, J. B., Zhang, Z. Y. & Yang, W. T. Synthesis and characterization of polyesteramides having short Nylon-6 segments in the main chains through polycondensation and chain extension. *Polymer* **52**, 6046–6055, doi:10.1016/j.polymer.2011.10.048 (2011).

24 Haussler, M., Eck, M., Rothauer, D. & Mecking, S. Closed-loop recycling of polyethylene-like materials. *Nature* **590**, 423–427, doi:10.1038/s41586-020-03149-9 (2021).

25 Koga, T., Morishita, T., Harumoto, Y., Nishimura, S. & Higashi, N. Spider silk-inspired peptide multiblock hybrid copolymers for self-healable thin film materials. *Mater Adv* **2**, 7851–7860, doi:10.1039/d1ma00823d (2021).

26 Kocen, A. L., Cui, S. L., Lin, T. W., LaPointe, A. M. & Coates, G. W. Chemically Recyclable Ester-Linked Polypropylene. *J Am Chem Soc* **144**, 12613–12618, doi:10.1021/jacs.2c04499 (2022).

27 Urciuoli, G. *et al.* Thermal Fractionation of Ethylene/1-Octene Multiblock Copolymers from Chain Shuttling Polymerization. *Macromolecules* **55**, 5656–5668, doi:10.1021/acs.macromol.2c00773 (2022).

28 Amamoto, Y. Data-driven approaches for structure-property relationships in polymer science for prediction and understanding. *Polym J* **54**, 957–967, doi:10.1038/s41428-022-00648-6 (2022).

29 Okazawa, K. *et al.* Exploring the Optimal Alloy for Nitrogen Activation by Combining Bayesian Optimization with Density Functional Theory Calculations. *ACS Omega* **49**, 45403–45408, doi:10.1021/acsomega.2c05988 (2022).

30 Kosuri, S. *et al.* Machine-Assisted Discovery of Chondroitinase ABC Complexes toward Sustained Neural Regeneration. *Adv Healthc Mater* **11**, 2102101, doi: 10.1002/adhm.202102101 (2022).

31 Tamasi, M. J. *et al.* Machine Learning on a Robotic Platform for the Design of Polymer-Protein Hybrids. *Adv Mater* **34**, 2201809, doi: 10.1002/adma.202201809 (2022).

32 Suh, J. S., Suh, B. C., Bae, J. H. & Kim, Y. M. Machine learning-based design of biodegradable Mg alloys for load-bearing implants. *Mater Design* **225**, 111442, doi: 10.1016/j.matdes.2022.111442 (2023).

33 Saito, Y. *et al.* Machine-Learning-Guided Mutagenesis for Directed Evolution of Fluorescent Proteins. *ACS Synth Biol* **7**, 2014–2022, doi:10.1021/acssynbio.8b00155 (2018).

34 Batra, R. *et al.* Machine learning overcomes human bias in the discovery of self-assembling peptides. *Nat Chem* **14**, 1427–1435, doi:10.1038/s41557-022-01055-3 (2022).

35 Terayama, K., Sumita, M., Tamura, R. & Tsuda, K. Black-Box Optimization for Automated Discovery. *Accounts Chem Res* **54**, 1334–1346, doi:10.1021/acs.accounts.0c00713 (2021).

36 Zamengo, M., Wu, S. P., Yoshida, R. & Morikawa, J. Multi-objective optimization for assisting the design of fixed-type packed bed reactors for chemical heat storage. *Appl Therm Eng* **218**, 119327, doi: 10.1016/j.applthermaleng.2022.119327 (2023).

37 Min, K., Cuiffi, J. D. & Mathers, R. T. Ranking environmental degradation trends of plastic marine debris based on physical properties and molecular structure. *Nat Commun* **11**, 727, doi: 10.1038/s41467-020-14538-z (2020).

38 Amamoto, Y., Kikutake, H., Kojio, K., Takahara, A. & Terayama, K. Visualization of

judgment regions in convolutional neural networks for X-ray diffraction and scattering images of aliphatic polyesters. *Polym J* **53**, 1269–1279, doi:10.1038/s41428-021-00531-w (2021).

39 Takamura, A., Tsukamoto, K., Sakata, K. & Kikuchi, J. Integrative measurement analysis via machine learning descriptor selection for investigating physical properties of biopolymers in hairs. *Sci Rep* **11**, 24359, doi: 10.1038/s41598-021-03793-9 (2021).

40 Wang, J. *et al.* Estimating the Relative Crystallinity of Biodegradable Polylactic Acid and Polyglycolide Polymer Composites by Machine Learning Methodologies. *Polymers* **14**, 527, doi: 10.3390/polym14030527 (2022).

41 Ryadnov, M. G. & Woolfson, D. N. Engineering the morphology of a selfassembling protein fibre. *Nat Mater* **2**, 329–332, doi: 10.1038/nmat885 (2003).

42 Tsuchiya, K., Ishii, T., Masunaga, H. & Numata, K. Spider dragline silk composite films doped with linear and telechelic polyalanine: Effect of polyalanine on the structure and mechanical properties. *Sci Rep* **8**, 3654, doi: 10.1038/s41598-018-21970-1 (2018).

43 Wu, J. H. *et al.* Rationally designed synthetic protein hydrogels with predictable mechanical properties. *Nat Commun* **9**, 620, doi: 10.1038/s41467-018-02917-6 (2018).

44 Gudeangadi, P. G. *et al.* Poly(alanine-nylon-alanine) as a bioplastic: chemoenzymatic synthesis, thermal properties and biological degradation effects. *Polym Chem* **11**, 4920–4927, doi:10.1039/d0py00137f (2020).

45 Tsuchiya, K. & Numata, K. Facile terminal functionalization of peptides by protease-catalyzed chemoenzymatic polymerization toward synthesis of polymeric architectures consisting of peptides. *Polym Chem* **11**, 560–567, doi:10.1039/c9py01335k (2020).

46 Hu, J. Y. *et al.* Design of synthetic collagens that assemble into supramolecular banded fibers as a functional biomaterial testbed. *Nat Commun* **13**, 6761, doi: 10.1038/s41467-022-34127-6 (2022).

47 Kinoshita, S. *et al.* Purification and Characterization of 6-Aminohexanoic-Acid-Oligomer Hydrolase of Flavobacterium Sp-Ki72. *Eur J Biochem* **116**, 547–551, doi: 10.1111/j.1432-1033.1981.tb05371.x (1981).

48 Tian, F. F., Zhou, P. & Li, Z. L. T-scale as a novel vector of topological descriptors for amino acids and its application in QSARs of peptides. *J Mol Struct* **830**, 106–115, doi:10.1016/j.molstruc.2006.07.004 (2007).

49 Aharoni, S. M. *n-Nylons: Their Synthesis, Structure, and Properties*. (John Wiley & Sons Ltd., 1997).

50 Peinemann, K. V., Abetz, V. & Simon, P. F. Asymmetric superstructure formed in a block copolymer via phase separation. *Nat Mater* **6**, 992–996, doi:10.1038/nmat2038 (2007).

51 Sakamoto, T. *et al.* Evaluation of dynamic features of Escherichia coli 16S ribosomal RNA in homogeneous physiological solution. *Biophys J* **89**, 4122–4128, doi:10.1529/biophysj.105.062455 (2005).

52 Vainio, M. J. & Johnson, M. S. Generating conformer ensembles using a multiobjective genetic algorithm. *J Chem Inf Model* **47**, 2462–2474, doi:10.1021/ci6005646 (2007).

53 Winmostar V11, X-Ability Co. Ltd., Tokyo, Japan, 2023.

54 Hariharan, P. C. & Pople, J. A. The influence of polarization functions on molecular orbital hydrogenation energies. *Theoretica chimica acta* **28**, 213–222, doi:10.1007/BF00533485 (1973).

55 Lee, C., Yang, W. & Parr, R. G. Development of the Colle-Salvetti correlation-energy formula into a functional of the electron density. *Physical Review B* **37**, 785–789, doi:10.1103/PhysRevB.37.785 (1988).

56 Becke, A. D. Density‐functional thermochemistry. III. The role of exact exchange. *The Journal of Chemical Physics* **98**, 5648–5652, doi:10.1063/1.464913 (1993).

57 Hehre, W. J., Ditchfield, R. & Pople, J. A. Self—Consistent Molecular Orbital Methods. XII. Further Extensions of Gaussian—Type Basis Sets for Use in Molecular Orbital Studies of Organic Molecules. *The Journal of Chemical Physics* **56**, 2257–2261, doi:10.1063/1.1677527 (2003).

58 Gaussian 16 Rev. C.01 (Wallingford, CT, 2016).

59 Tomasi, J., Mennucci, B. & Cammi, R. Quantum mechanical continuum solvation models. *Chem Rev* **105**, 2999–3093, doi:10.1021/cr9904009 (2005).

60 Motoyama, Y. *et al.* Bayesian optimization package: PHYSBO. *Comput Phys Commun* **278**, 108405, doi: 10.1016/j.cpc.2022.108405 (2022).

61 Couckuyt, I., Deschrijver, D. & Dhaene, T. Fast calculation of multiobjective probability of improvement and expected improvement criteria for Pareto optimization. *J Global Optim* **60**, 575–594, doi:10.1007/s10898-013-0118-2 (2014).

62 Yahyaa, S. M., B. Thompson Sampling for Multi-Objective Multi-Armed Bandits Problem. *Proc. Eur. Symp. Artif. Neural Netw., Comput. Intell. Mach. Learn.*, 47–52 (2015).

63 Hoerl, A. E. & Kennard, R. W. Ridge regression: Biased estimation for nonorthogonal problems. *Technometrics* **42**, 80–86, doi: 10.2307/1271436 (2000).

64 Tibshirani, R. Regression shrinkage and selection via the Lasso. *J Roy Stat Soc B* **58**, 267–288, doi: 10.1111/j.2517-6161.1996.tb02080.x (1996).

65 Ferri, F. J., Pudil, P., Hatef, M. & Kittler, J. in *Machine Intelligence and Pattern Recognition* Vol. 16 (eds Edzard S. Gelsema & Laveen S. Kanal) 403–413 (North-Holland, 1994).

Figures

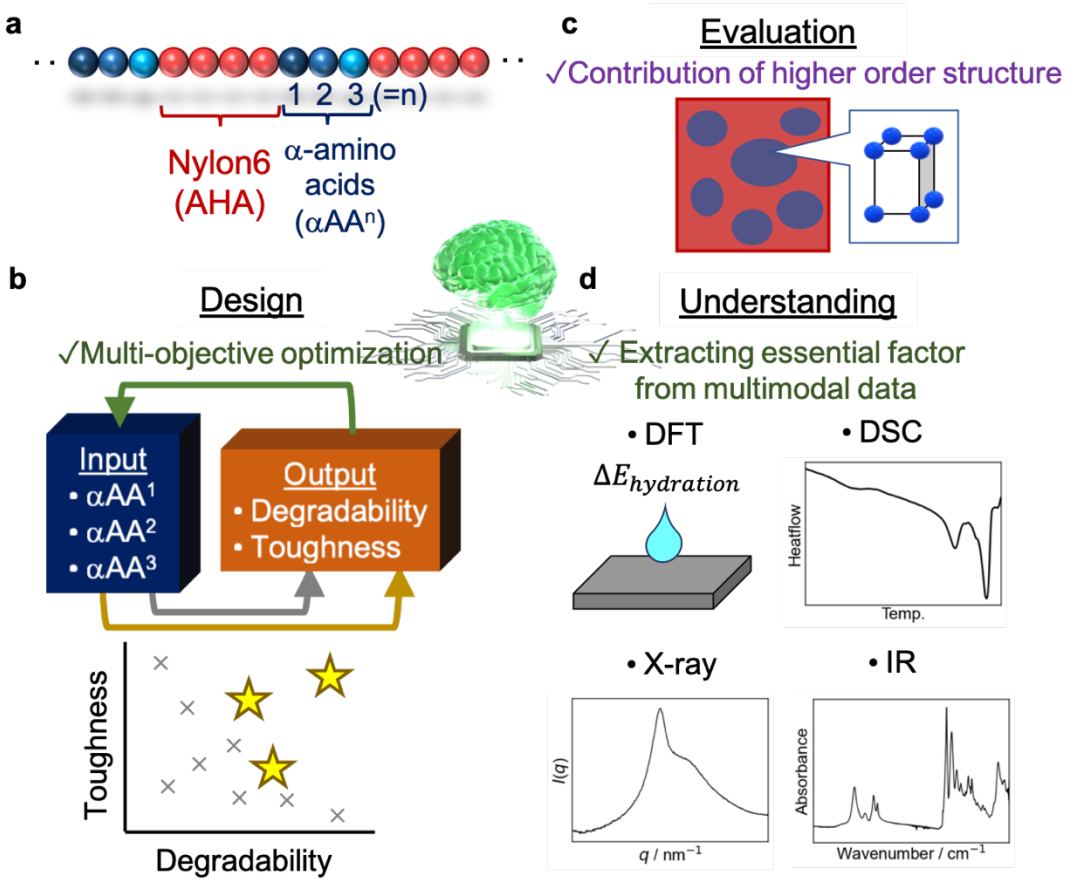

Fig. 1 Schematic representation of this work. a, Multiblock polyamide consisting of AHA and αAA segments. **b**, Multi-objective polyamide optimisation for degradability and toughness. **c**, Evaluating the material properties of higher-order polyamide structures. **d**, Extracting important property factors from experimental/calculational data.

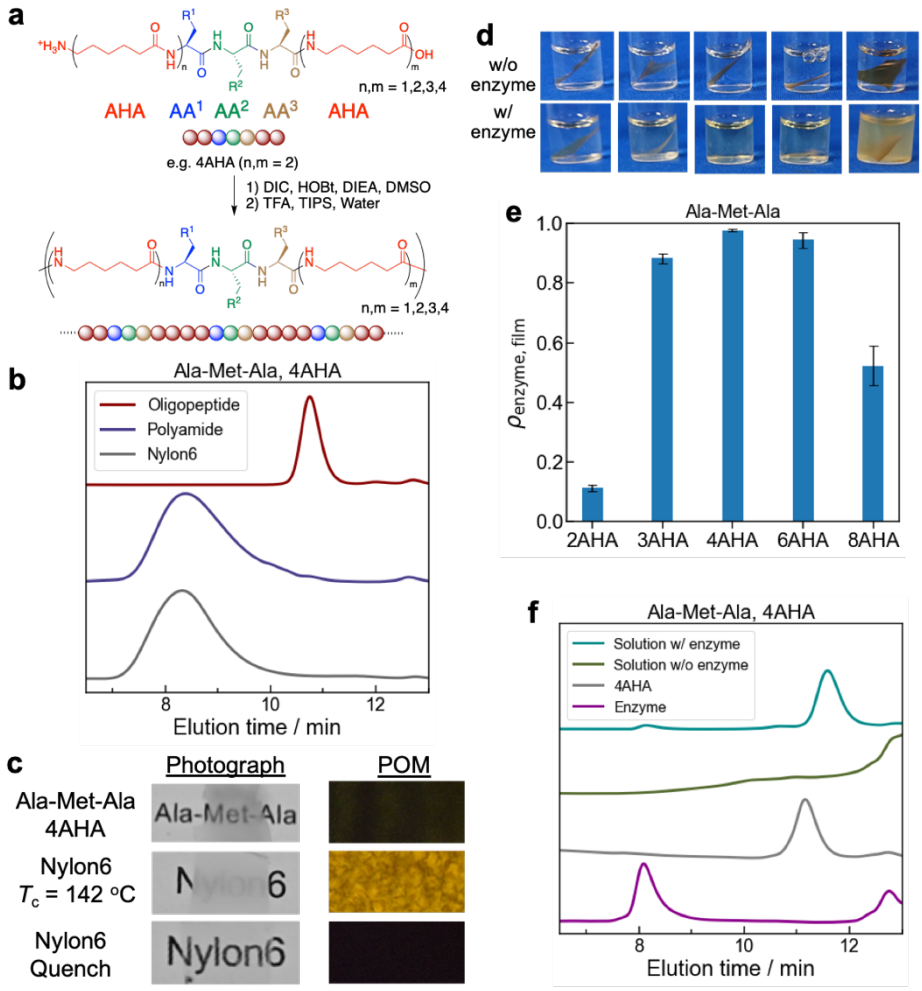

Fig. 2 Polyamide preparation and enzymatic degradability. a, Multiblock polyamide synthesis by coupling an oligopeptide composed of AHA and αAA units. **b**, GPC traces for Nylon6 and the polyamide before and after coupling. **c**, Photographic images and polarised optical microscopy (POM) images of Nylon6 and a polyamide composed of Ala-Met-Ala. **d**, Photographic images and **e**, enzymatic degradation rates of polyamide films ($\rho_{\text{enzyme, film}}$) after 2 d in a buffer solution of Proteinase K. **f**, GPC traces for reaction products with/without enzymes, 4AHA, and enzymes.

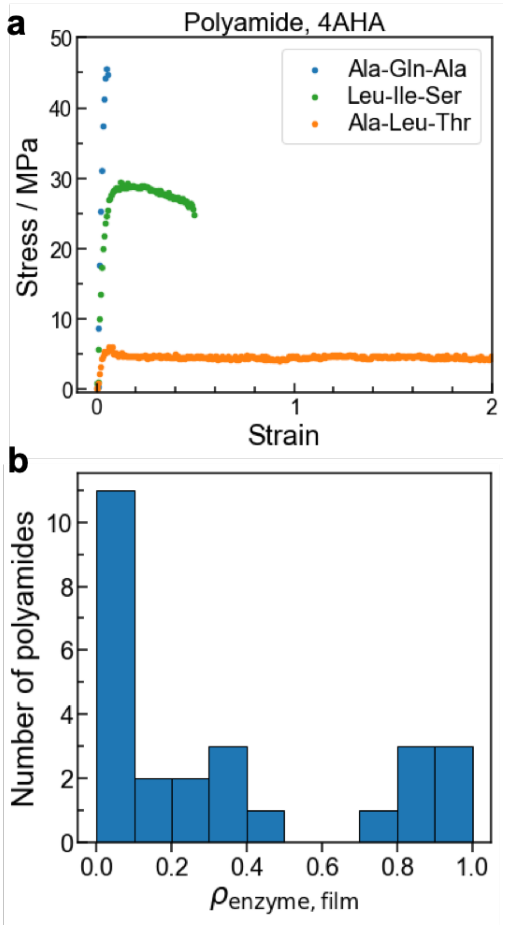

Fig. 3 Properties of polyamide films with several α-amino acid sequences. a, Stress–strain curves of representative polyamide films at room temperature. **b**, Enzymatic degradation rates of polyamide films ($\rho_{\text{enzyme, film}}$) with several αAA sequences.

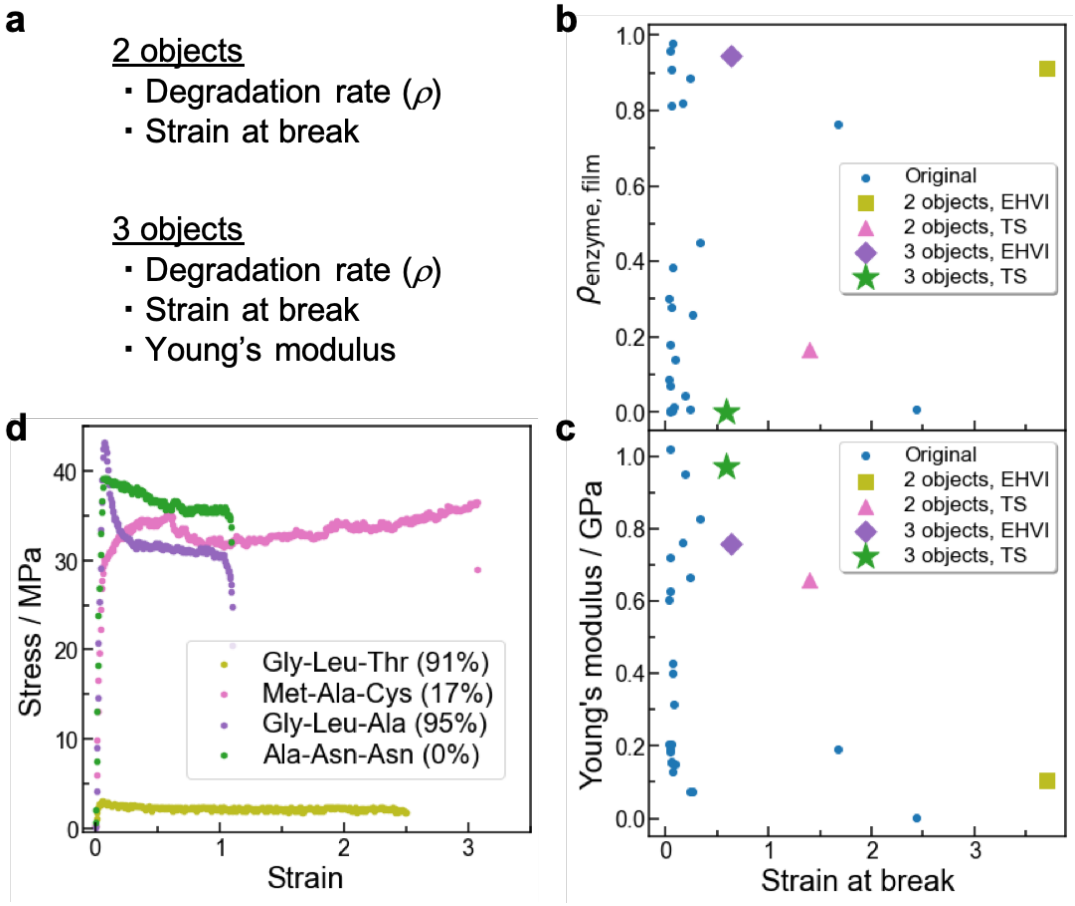

Fig. 4 Multi-objective polyamide optimisation for toughness and degradability using BO. **a**, Target properties for the multi-objective optimisation. **b-c**, Multi-objective optimisation results for polyamide films in terms of $\rho_{\text{enzyme, film}}$, Young' modulus, and strain at break. **d**, Stress–strain curves for polyamide films with sequences suggested by BO; $\rho_{\text{enzyme, film}}$ values are shown in parentheses.

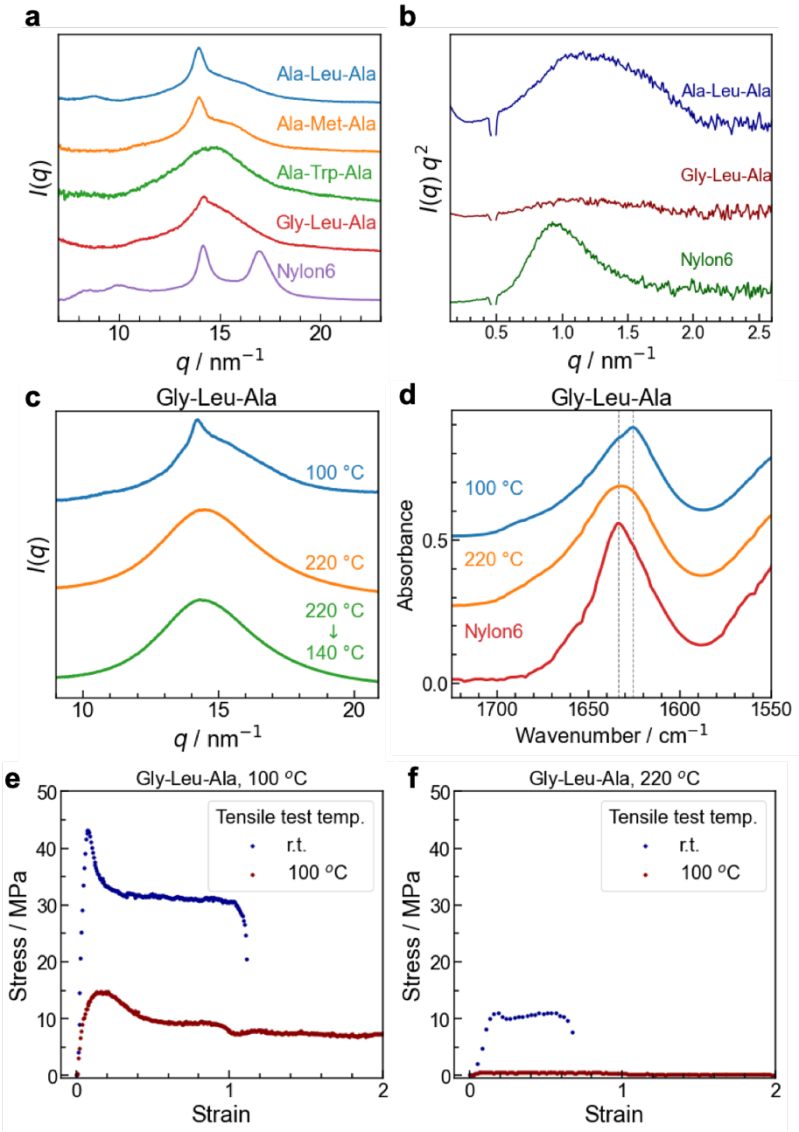

Fig. 5 Multiblock polyamide phase separation and its effect on mechanical properties. **a**, WAXS profiles of polyamide films with different αAA sequences and 4AHA units. **b**, Kratky plots of SAXS data for Nylon6 and polyamides with different sequences. **c-d**, (**c**) WAXS profiles and (**d**) IR spectra of Nylon6 and a thermally treated polyamide containing Gly-Leu-Ala sequences and 4AHA units, with annealing temperatures listed. Stress–strain curves for a Gly-Leu-Ala-containing polyamide thermally treated at **e**, 100 °C and **f**, 220 °C. Tensile testing was carried out at room temperature or 100 °C.

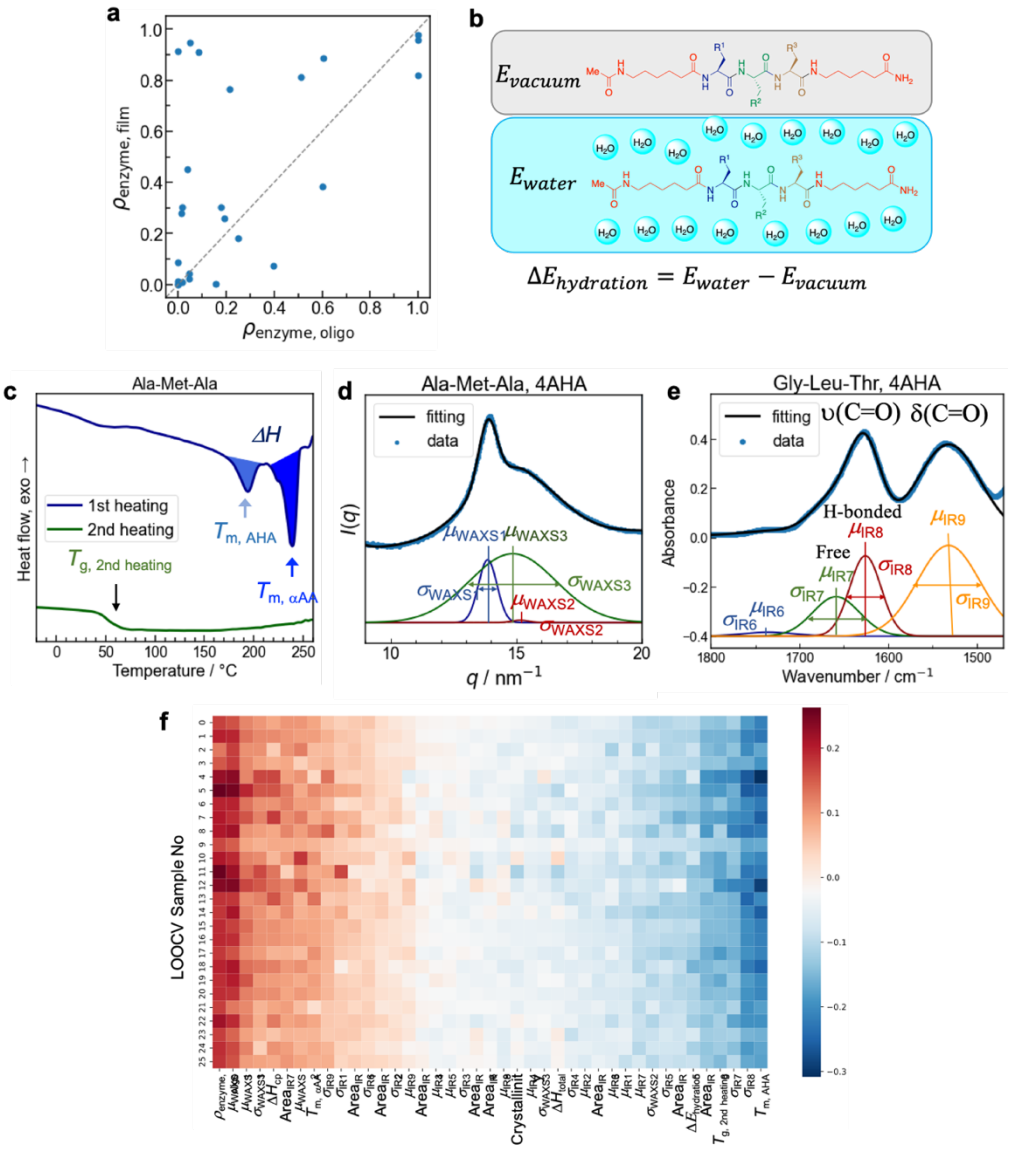

Fig. 6 Higher-order structures essential for degradability. a, Relationships between the enzymatic degradabilities of polyamides in their film states ($\rho_{enzyme,\ film}$) and corresponding oligopeptides ($\rho_{enzyme,\ oligo}$) with several αAA sequences. **b**, Evaluating hydration energies based on quantum-chemical calculations. Extracting physical values from **c**, DSC, **d**, WAXS, and **e**, IR data. Gaussian distributions were used to peak-fit the IR and WAXS data. **f**, Heatmap of ridge regression analysis coefficients for different LOOCV test samples (vertical direction) and various physical values (horizontal direction). Coefficients are reflected by the colour bar.

SUPPLEMENTARY INFORMATION

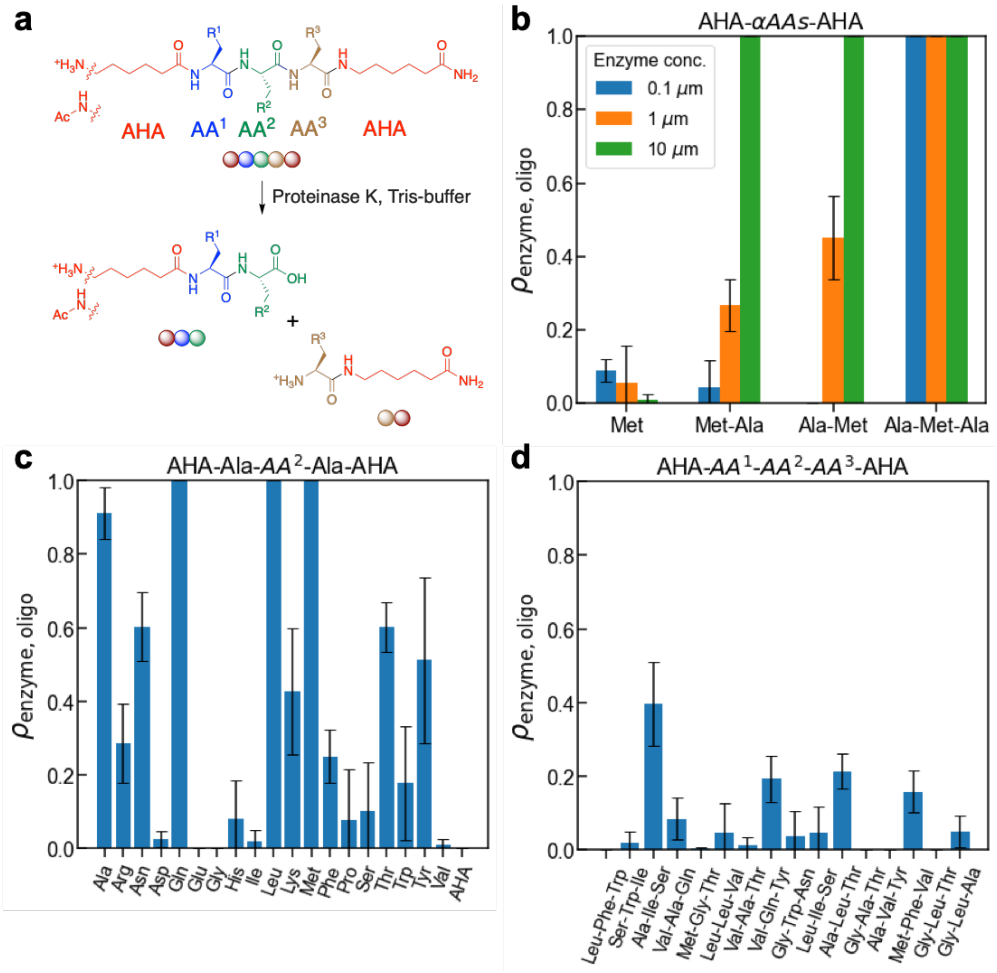

Supplementary Fig. 1 Oligopeptide enzymatic degradation. **a**, Schematic representation of an oligopeptide with three αAAs sandwiched by AHAs and cleaved by Proteinase K in Tris buffer. **b**, Enzyme-concentration-dependence of the degradation rate ($\rho_{\text{enzyme, oligo}}$) for oligopeptides with Met and Ala units. **c-d**, Degradation rates of oligopeptides ($\rho_{\text{enzyme, oligo}}$) with several αAA sequences.

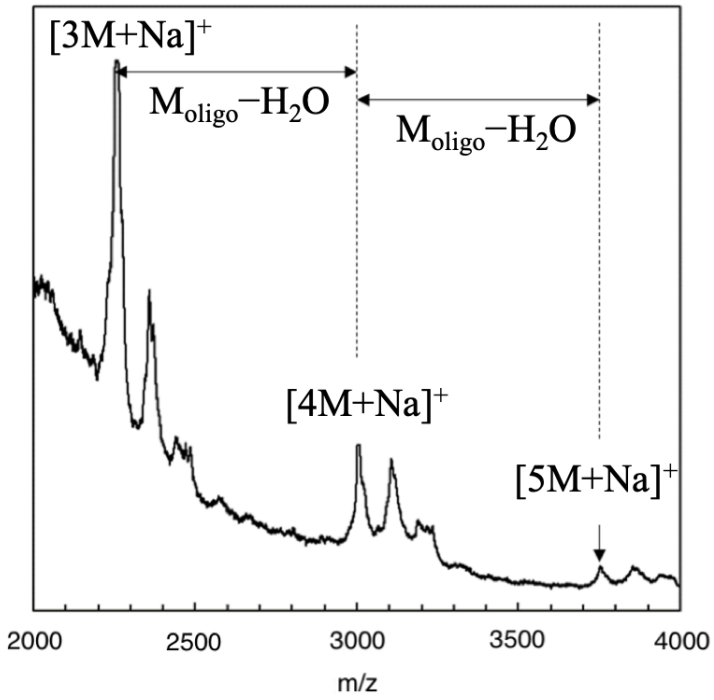

Supplementary Fig. 2 MALDI-TOF-MS spectrum of a polyamide with the Ala-Phe-Ala sequence and 4AHA units. M_{oligo} corresponds to the molecular weight of the precursor oligopeptide.

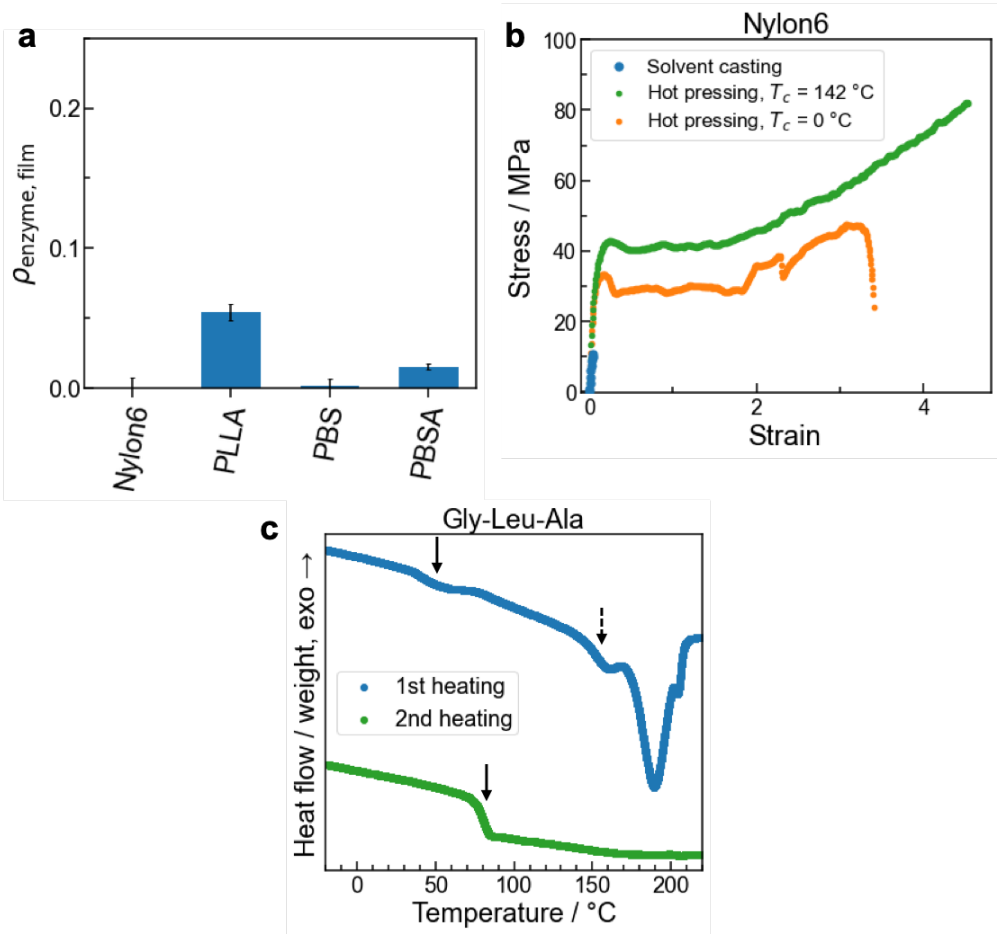

Supplementary Fig. 3 Properties of a polyamide and representative biodegradable polymers. **a**, Degradation rates of Nylon6, poly(lactic acid) (PLLA), polybutylene succinate (PBS), and polybutylene succinate-co-adipate (PBSA). **b**, Stress–strain curves for Nylon6 obtained by elongation testing at room temperature. Nylon6 was prepared under several conditions. **c**, DSC curves of polyamide films containing Gly-Leu-Ala sequences and 4AHA units.

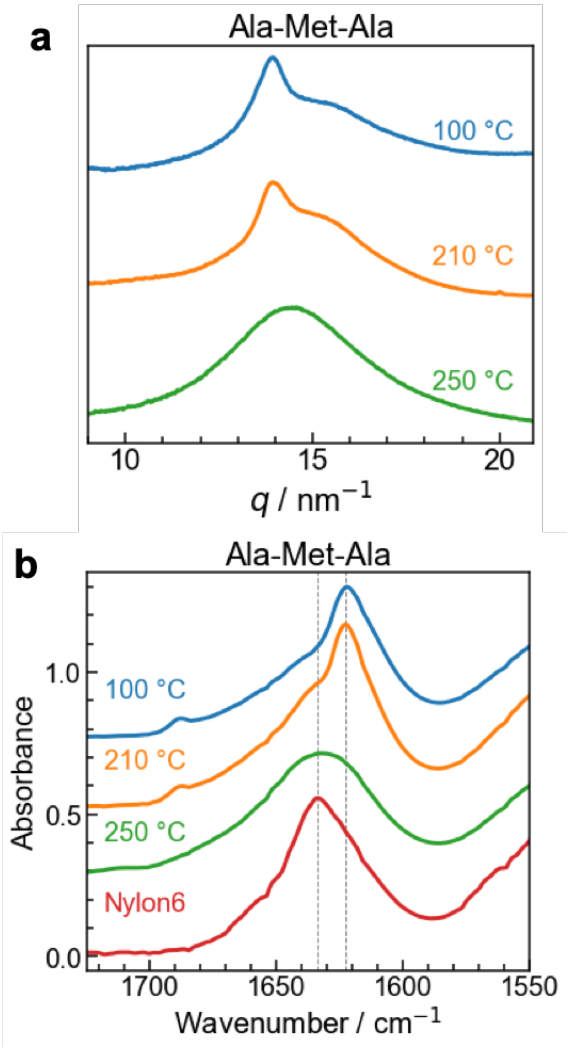

Supplementary Fig. 4 Change in the higher order structure of a polyamide film during thermal treatment. a, WAXS profiles and **b,** IR spectra of annealed Ala-Met-Ala-containing polyamide at 100, 210, and 250 °C and Nylon6. These data were acquired at room temperature.

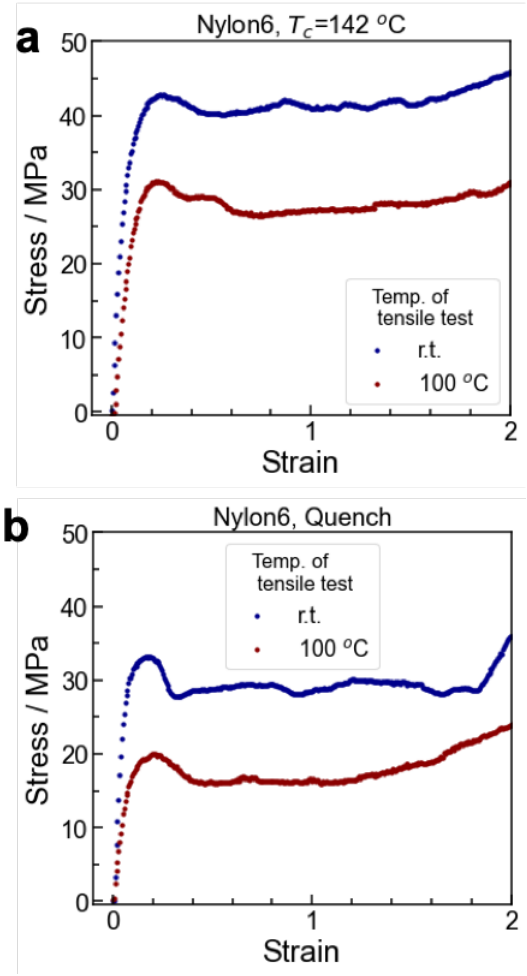

Supplementary Fig. 5 Stress-strain curves for Nylon6 with different thermal histories while heated. Stress–strain curves for Nylon6 **a**, crystallised at 142 °C and **b**, a quenched sample. T_c is the crystal temperature of Nylon6. The quenched sample was treated using ice water without crystallisation. Tensile testing was carried out at room temperature or 100 °C.

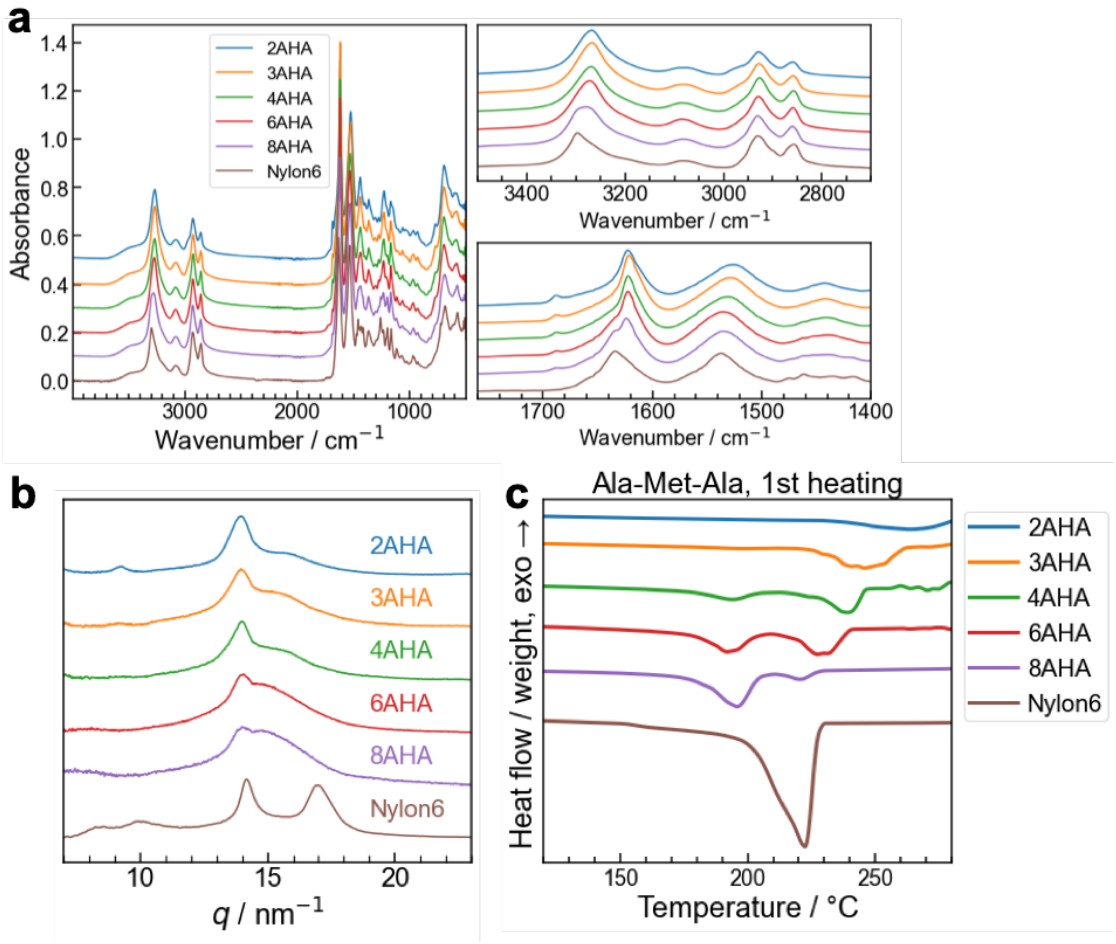

Supplementary Fig. 6 a, IR spectra, b, WAXS profiles, and c, DSC traces for Nylon6 and polyamides with different numbers of AHA units. The αAA sequence in the polyamide was fixed to be Ala-Met-Ala.

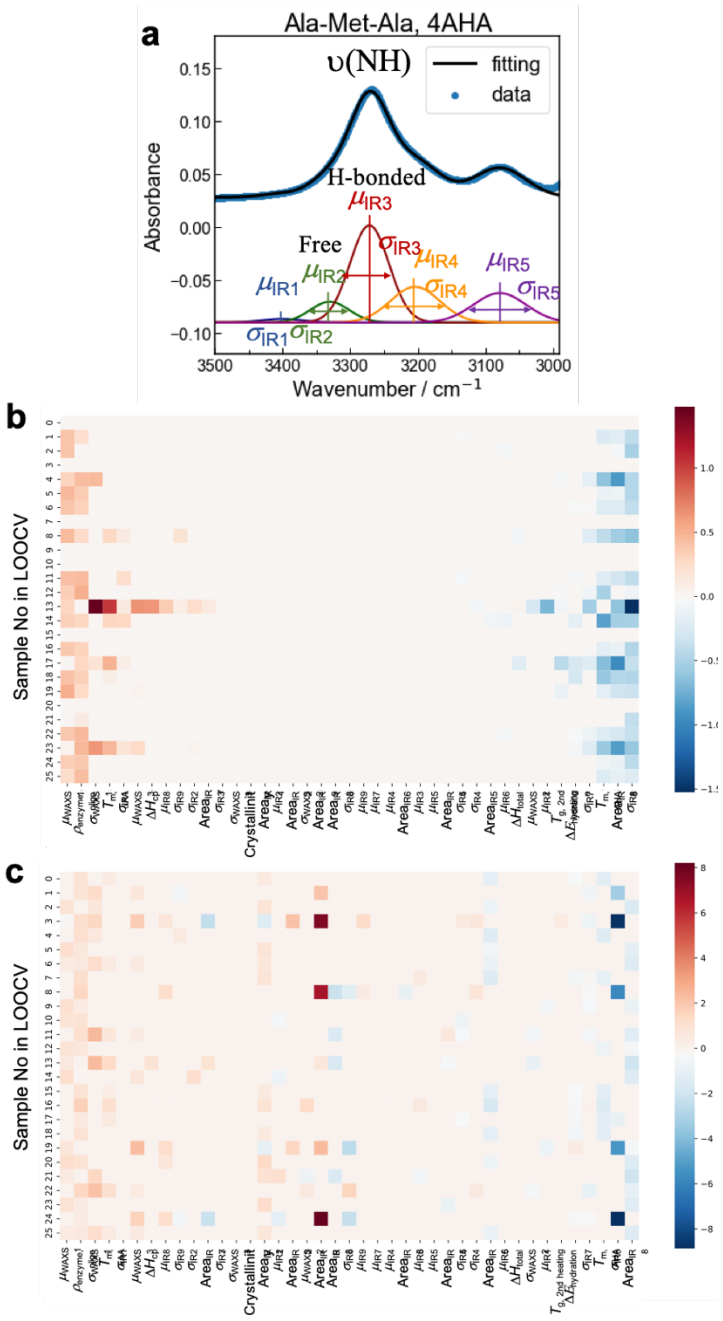

Supplementary Fig. 7 Extracting feature values from IR spectra and heatmaps of important physical values. The colour bars in the heatmaps correspond to **b,** LASSO and **c,** SFS-based multilinear regression coefficients. Vertical and horizontal directions correspond to different LOOCV test samples and various physical values, respectively.

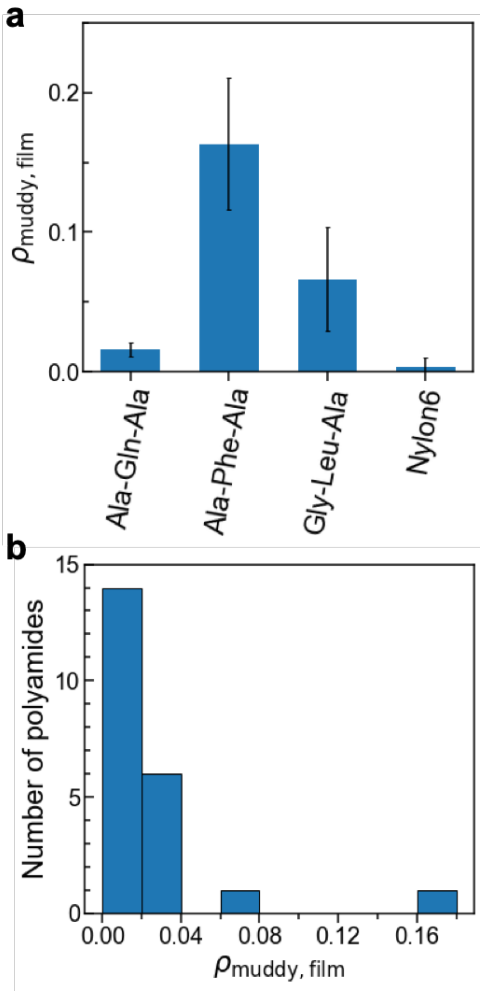

Supplementary Fig. 8 Polyamide degradation in a natural environment. **a**, Degradation rates in muddy water ($\rho_{\text{muddy, film}}$) for representative polyamide films and Nylon6. The error bars correspond to standard deviations for four measured values. **b**, histogram of $\rho_{\text{muddy, film}}$ for polyamides with different αAA sequences.